HHS Public Access

Author manuscript

Matrix Biol. Author manuscript; available in PMC 2024 June 01.

Published in final edited form as:

Matrix Biol. 2023 June ; 120: 43–59. doi:10.1016/j.matbio.2023.05.002.

CaMKII inhibition due to TRIC-B loss-of-function dysregulates SMAD signalling in osteogenesis imperfecta

Roberta Besio[1], **Barbara M. Contento**[1], **Nadia Garibaldi**[1], **Marta Filibian**[2,3], **Stephan Sonntag**[4,5], **Doron Shmerling**[4], **Francesca Tonelli**[1], **Marco Biggiogera**[6], **Marisa Brini**[7,8], **Andrea Salmaso**[7], **Milena Jovanovic**[9], **Joan C. Marini**[9], **Antonio Rossi**[1], **Antonella Forlino**[1,*]

[1]Department of Molecular Medicine, Biochemistry Unit, University of Pavia, Pavia, 27100, Italy

[2]Centro Grandi Strumenti, University of Pavia, 27100, Pavia, Italy

[3]INFN, Istituto Nazionale di Fisica Nucleare-Pavia Unit, Pavia, 27100, Italy

[4]PolyGene AG, 8153 Rümlang, Switzerland

[5]LIMES-Institute, University of Bonn, 53115, Bonn, Germany

[6]Department of Biology and Biotechnology, University of Pavia, 27100, Pavia, Italy

[7]Department of Biology, University of Padova, Padova, Italy

[8]Centro Studi per la Neurodegenerazione (CESNE), University of Padova, Padova, Italy

[9]Section on Heritable Disorders of Bone and Extracellular Matrix, Eunice Kennedy Shiver National Institute of Child Health and Human Development, National Institute of Health, Bethesda, MD, USA

Abstract

Ca^{2+} is a second messenger that regulates a variety of cellular responses in bone, including osteoblast differentiation. Mutations in trimeric intracellular cation channel B (TRIC-B), an endoplasmic reticulum channel specific for K^{+}, a counter ion for Ca^{2+} flux, affect bone and cause a recessive form of osteogenesis imperfecta (OI) with a still puzzling mechanism. Using a conditional *Tmem38b* knock out mouse, we demonstrated that lack of TRIC-B in osteoblasts strongly impairs skeleton growth and structure, leading to bone fractures. At the cellular level, delayed osteoblast differentiation and decreased collagen synthesis were found consequent to the Ca^{2+} imbalance and associated with reduced collagen incorporation in the extracellular

*Corresponding Author: Antonella Forlino, PhD, Professor of Biochemistry, Department of Molecular Medicine, Biochemistry Unit, University of Pavia, Via Taramelli 3B, 27100, Pavia, Italy, Fax: +39-0382-423108, aforlino@unipv.it.

Author contribution

AF and RB designed the experiments. RB and BMC performed experiments and analyzed the results. NG, MF, SS, DS, MB, AS, MJ performed specific experiments. MB and JCM analyzed specific results. RB and AF wrote the manuscript with helpful revision by AR, FT, JCM. All the authors have read and approved the manuscript.

Declaration of Competing Interest

The authors have declared that no conflict of interest exists.

matrix and poor mineralization. The impaired SMAD signalling detected in mutant mice, and validated in OI patient osteoblasts, explained the osteoblast malfunction. The reduced SMAD phosphorylation and nuclear translocation were mainly caused by alteration in Ca^{2+} calmodulin kinase II (CaMKII)-mediated signalling and to a less extend by a lower TGF-β reservoir. SMAD signalling, osteoblast differentiation and matrix mineralization were only partially rescued by TGF-β treatment, strengthening the impact of CaMKII-SMAD axes on osteoblast function. Our data established the TRIC-B role in osteoblasts and deepened the contribution of the CaMKII-SMAD signalling in bone.

Keywords

TRIC-B; bone; collagen; osteogenesis imperfecta; osteoblast; murine model

Introduction

The ubiquitous trimeric intracellular cation channel B (TRIC-B), encoded by *TMEM38B*, is a rough endoplasmic reticulum (rER) integral membrane protein acting as monovalent cation-specific channel for K^+ ions, modulating intracellular Ca^{2+} flux (1–4). Ca^{2+} has a crucial role in regulating many aspects of physiological responses by acting as second messenger for several cellular biological processes, ranging from differentiation/proliferation to metabolism (5). To enable these multiple responsive behaviors, the cytosolic Ca^{2+} concentration is kept extremely low through sequestration into intracellular stores, thus allowing quick and transient Ca^{2+} spikes upon stimulation of voltage or ligands Ca^{2+}-permeable channels (6–8). Ca^{2+} signals can occur as single transients, as oscillations, or as a sustained plateau, and this triggers the differential activation and/or inhibition of downstream mediators that determine the type, the strength and the specificity of the signal response. The rapid change in cytosolic concentration is responsible for the activation of Ca^{2+} dependent proteins and/or enzymes, that mediates cellular response to external signals (9). In this context, the K^+ ions influx though the TRIC-B channel participates in counterbalancing the Ca^{2+} exit from the rER and thus, likely, the subsequent Ca^{2+}-regulated cellular events.

In bone, at the tissue level, osteoblasts (OBs) and osteoclasts maintain skeletal integrity and systemic Ca^{2+} homeostasis through remodeling that is finely regulated by means of hormones, cytokines and matrix embedded factors (10, 11), while, at the cellular level, Ca^{2+} plays a key role in osteoblastogenesis (12–16).

Mutations in *TMEM38B* cause the autosomal recessive osteogenesis imperfecta (OI) type XIV (OMIM #615066). In affected individuals the skeletal phenotype is predominantly moderate although quite variable even in the same family (17), including bone fracture risk and secondary cardiac and muscle features. OI is a heterogeneous collagen type I-related group of monogenic diseases characterized by impairment in collagen amount, synthesis, post translational modification, secretion and/or extracellular processing and altered osteoblast differentiation and function, all sharing skeletal abnormalities. Individuals with OI are generally characterized by growth delay, low bone mass, bone fragility and

frequent fractures often not associated with trauma, while extra skeletal features have variable penetrance (18). Over the past few decades, the identification of several causal genes for OI has not only improved precise diagnosis and genetic counselling of the disease, but also continuously driven the research of molecular mechanisms of bone formation and regulation of the skeletal system and the exploration of innovative therapies for bone-related diseases (19, 20). The identification of TRIC-B loss-of-function mutations in OI patients and of a bone phenotype in the global TRIC-B knock out (KO) mouse demonstrated the unexpected and relevant role for this ubiquitous channel in bone homeostasis (21). Bone fragility in absence of TRIC-B was associated with matrix insufficiency and to an alteration in the expression of several Ca^{2+} dependent proteins and enzymes involved in collagen folding and post translational modifications such as protein disulfide isomerase, known to have a role in α(I) chain recognition, proline hydroxylase and lysine hydroxylase 1 and 2, relevant for proline hydroxylation and helical and telopeptide lysine hydroxylation, respectively (22). Of note, TRIC-B KO mice die in the perinatal period due to insufficient surfactant production in the alveoli, limiting the use of the model to investigate the role of TRIC-B in the bone tissue (2, 21).

To define the molecular mechanism underlying OI type XIV, we generated an osteoblast specific conditional knock-out murine model of *Tmem38b* (*Runx2Cre;Tmem38b*$^{fl/fl}$). The model unraveled the TRIC-B role in osteoblasts and showed for the first time that the altered Ca^{2+} flux impairs Ca^{2+} calmodulin kinase II (CaMKII) dependent SMAD signalling, impacting skeleton growth and structure. The clarification of how altered Ca^{2+} flux translates into a low bone mass phenotype deepened our understanding of bone biology.

Results

TRIC-B deficiency in osteoblasts (OBs) causes bone deformity and bone fragility

Ubiquitous lack of TRIC-B in humans and mice is associated with osteogenesis imperfecta (OI). To determine the bone tissue-specific role of TRIC-B channel, we generated a *Tmem38b-flox* mouse that we mated with an OB-specific Cre transgenic mouse line (*Runx2Cre*) obtaining the conditional knock-out (*Runx2Cre; Tmem38b*$^{fl/fl}$, cKO) mouse (Supplementary Fig. 1A–F, Supplementary Fig. 2A). Efficacy and specificity of Cre recombination was assessed by qPCR on DNA extracted from decalcified bone and from a soft tissue (liver). Normal level of exon 3 containing WT allele was found in control mice bone (100 ± 7.8 %) and in liver from cKO mice (114 ± 5.6%), whereas only 3.1 ± 0.99 % was detected in cKO bone. Accordingly, a very low *Tmem38b* mRNA expression was detected in bone from cKO mice (Ctrl 1.00±0.39%; cKO 0.27±0.23). The exon 3 deletion resulting in a frameshift responsible for a premature stop codon at AA100 (Supplementary Fig. 2B) caused the absence of TRIC-B in cKO specifically in bone (Supplementary Fig. 2C). The cKO mouse was deeply phenotyped (Fig. 1).

At birth, mutant pups were undistinguishable from control, but growth delay was evident starting from day 7 in both sexes and became worse with age (Fig. 1A, B). 91.6% female and 82% male mutants died within the first 38 days of life (Supplementary Fig. 2D). In cKO animals alcian blue and alizarin red staining of whole skeleton at P28 revealed several deformities, the presence of calli in long bones and ribs (Fig. 1C) and a delay in the

vertebrae and skull ossification (Fig. 1D). X-ray imaging at the same age confirmed the severe bone deformations and calli indicative of previous spontaneous fracture healing (Fig. 1E, F). The micro computed tomography 3D reconstruction of the tibia showed shorter bone with a less tubular shape (Fig. 1G, H, I) and alterations in both the trabecular and the cortical compartments (Fig.2A, B) in cKO compared to control littermates, as supported by Alcian Blue Hematoxylin histological analysis on tibial distal metaphysis (Fig.2C).

Picro-sirius red staining clearly showed a disordered organization of the collagenic matrix in the cortical bone with clusters of thicker fibril bundle (Fig.2D). Bone geometrical properties were evaluated excluding deformed and fractured bones since the presence of calli could affect the bone parameters. At the trabecular level, bone volume/total volume, intersection surface, trabecular thickness, and bone mineral density (BMD) were significantly reduced in cKO mice compared to controls (Fig. 2E). Similarly, in the cortical compartment, bone volume, intersection surface and cortical thickness were significantly reduced in mutant mice, compatible with a phenotype of osteogenesis imperfecta. By contrast, the bone surface/bone volume ratio was higher in cKO mice, indicating an increased surface in mutant bone (Fig. 2F).

TRIC-B deficiency affects OB differentiation and matrix mineralization

The impact of loss of TRIC-B function on OB differentiation was investigated in primary calvarial cKO osteoblasts. Expression of osteoblastogenic genes was examined after 4, 10, 14 and 21 days of culture. The early osteoblast marker osterix (*Osx*) and the downstream genes alkaline phosphatase (*Alp*) and osteocalcin (*Bglap*) were downregulated (Fig. 3A), suggesting an impaired differentiation of precursor cells towards osteoblast lineage in mutant animals. The mineral deposition was also defective in the *Tmem38b* mutant cells (Fig. 3B), in a context of normal cell proliferation (Fig 3C). The impaired bone formation ability was further confirmed by the decreased activity of the ALP enzyme in mutant cells (Fig. 3D). A decreased expression of *Bglap* was confirmed *in vivo* in femur from *Tmem38b* mutant mice (Fig. 3E).

TRIC-B deficiency causes a decreased collagen synthesis and a reduced collagen incorporation into the matrix

In agreement with findings in the TRIC-B global knock out model (21), enlargement of ER cisternae was detected by electron microscopy in mutant osteoblasts (Fig. 4A). Double membranes vacuoles, supporting autophagosome formation, were also found in cKO animals. Analyses of ER proteostasis, following treatment of cells with the protein aggregate-binding fluorescent molecule Thioflavin T (ThT) (23), showed enhanced fluorescence in mutant OBs compared to controls, indicating the intracellular accumulation of misfolded material (Fig. 4B). Reduced total protein synthesis (Fig. 4C), as well as reduced collagen synthesis both at the mRNA and protein level (Fig. 4D, E), were detected in the mutants. Furthermore, the matrix incorporation of collagen I was significantly decreased (Fig 4F). The protein level of HSP47, the ER chaperone known to play a key role in collagen folding and secretion (24), was significantly increased in mutant OBs (Fig. 4 G). Electrophoretic analysis of collagen extracted form bone revealed a faster migration

of α(I) bands respect to control supporting reduced post translational modifications, i.e. hydroxylation and glycosylation (Fig. 4H), as reported in OI patients' cells (22).

TRIC-B deficiency reduces Ca^{2+} calmodulin kinase II phosphorylation

It has been reported both in patients' cells and in global knockout mice that TRIC-B deficiency alters intracellular Ca^{2+} flux, reducing Ca^{2+} transients from the ER upon an inositol trisphosphate receptor-generating (IP_3R) agonist stimulation (21, 22). To characterize Ca^{2+} signalling in cKO OBs, we measured both global cytosolic and mitochondrial Ca^{2+} transients induced upon cell stimulation with an IP_3R agonist that releases Ca^{2+} from the ER. In cKO cells, in presence of normal cytosolic Ca^{2+} transients (Fig. 5A), we found reduced Ca^{2+} transients in mitochondria (Fig. 5B), possibly reflecting an impairment in Ca^{2+} efflux from the ER, as reported in patients and global KO mouse, and a consequent reduction of the Ca^{2+} microdomains entity at the site of release.

Given the relevance of Ca^{2+} for the activation of CaMKII, essential for promoting early differentiation of osteoprogenitors, pathway activation was examined. While, as expected, CaMKII activity in mutant cells lysates supplemented with external Ca^{2+} was unchanged (Supplementary Fig. 3A), a reduction of the threonine 286 phosphorylated form of CaMKII was found in cKO OBs (Fig. 5C).

TRIC-B deficiency decreases SMAD signalling pathway mainly thought Ca^{2+} calmodulin kinase

A significant reduction in the phospho SMAD2 and 3 (pSMAD2 and 3) proteins was found in mutant OBs in the presence of an unchanged SMAD2/3 level (Fig. 5D, E, F). Importantly, a significant decrease of pSMAD2 was confirmed *in vivo* in mutant bone (Fig. 5G), together with a decreased transcript expression of the TGF-β target gene *Cdkn1a* (Fig. 5H).

Since the SMAD2/3 proteins are the direct targets of TGF-β and we detected matrix insufficiency, likely affecting the TGB-β reservoir, TGF-β level was assessed. In mutant samples, TGF-β was decreased at the protein level, while a normal transcript level was found (Fig. 6A, B).

To dissect the functional link between SMAD signalling activation, Ca^{2+} dependent CaMKII activity and TGF-β in OBs, we measured in primary murine control and cKO cells the effect of the CaMKII inhibitor KN93 on pSMAD3 level in the absence or presence of exogenous TGF-β (Fig. 6C, D). In both control and cKO cells, pSMAD3 level was increased following TGF-β stimulation and, of note, this effect was significantly reduced by KN93 pointing to a dependence of SMAD activation on CaMKII (Fig. 6C, D). The decreased level of pSMAD3 in cKO compared to control cells upon TGF-β stimulation indicated the CaMKII signalling impairment. Importantly, without TGF-β treatment, KN93 significantly reduced pSMAD3 level in control while did not affect cKO cells, confirming that CaMKII activity is already compromised as a consequence of the lack of TRIC-B (Fig. 6C, D).

Total pSMAD3 level, pSMAD nuclear localization (Fig. 6E, F, G) as well as osteoblasts differentiation and mineralization of mutant calvaria cells were only partially rescued by a

short term TGF−β stimulation (Fig. 6H, I and Supplementary Fig. 3B), further supporting the impact of CaMKII-SMAD axes on osteoblast function.

Impaired SMAD signalling was confirmed in a *TMEM38B*-null OI XIV patient

To validate murine data on humans, the pSMAD level was investigated in primary OBs from a *TMEM38B*-null OI XIV patient with a severe phenotype and compared to a healthy age-matched control. A decreased protein level of pSMAD3 was found in *TMEM38B*-null patient OBs (Fig. 7), after stimulating cells with recombinant TGF-β, confirming the mechanistic importance of the murine finding.

Discussion

Osteoblast (OB) differentiation is a complex process that requires the activation of several transduction pathways in which Ca^{2+} represents a relevant second messenger (25). In our study we demonstrated that the bone alterations caused by the lack of the TRIC-B channel in OBs are due to a decreased SMAD pathway triggered by alteration in CaMKII-mediated signalling consequent to the abnormal Ca^{2+} flux (Fig. 8).

Ca^{2+} binding protein calmodulin (CaM), upon binding to Ca^{2+}, interacts and activates various target proteins including the serine/threonine kinase CaMKII, one of the main effector enzymes involved in Ca^{2+} signaling in eukaryotic cells (14). The binding produces a conformational change which, upon autophosphorylation at threonine 286, leads to the phosphorylation of CaMKII substrates (26–30).

CaMKII is thought to be a major decoder of Ca^{2+} oscillation since its kinase activity reflects the size and frequency of Ca^{2+} spikes (31). Indeed, an altered Ca^{2+} flux was found in patients with the low bone mass disorder osteogenesis imperfecta due to mutations in the rER membrane K^+ channel TRIC-B (22) and in a global knock out TRIC-B murine model (21), where also an increased calcium concentration in the ER was found. In OI patients' cells, in human foetal OBs (hFOB) knocked-out for *TMEM38B* and in the global *TRIC-B KO* mouse, collagen secretion and matrix mineralization were reduced, pointing to the relevance of TRIC-B in osteoblast activity (22, 32). Importantly, impaired bone mineralization was also confirmed in tric-b KO zebrafish larvae (33).

To dissect TRIC-B function in OB, we generated an OB specific TRIC-B conditional knock-out murine model (cKO) that reproduces the loss-of function of TRIC-B found in OI patients caused by deletions or missense mutations (22, 34–38). The severe skeletal phenotype of the cKO model demonstrated a cell intrinsic defect in OBs and thus the primary function of TRIC-B for bone development. The cKO phenotype positions itself in the more severe range described for OI type XIV patients. The high fracture frequency found in TRIC-B cKO mice long bones is likely responsible for motor disadvantage while the rib cage fractures likely harm internal organs, possibly explaining the lower survival expectancy.

In agreement with patients' cells and TRIC-B KO mouse and zebrafish data (21, 22, 33), ER cisternae enlargement was detected in cKO cells, together with reduced collagen secretion, supporting the presence of impaired cell homeostasis. In cKO, intracellular

proteins accumulation and increased levels of the collagen chaperone HSP47, the latter described also in tric-b KO zebrafish, were found, pointing to an intracellular collagen accumulation as detected in mature ALP-positive osteoblasts from KO mice (21).

The availability of the new surviving model allowed study of bone properties as well as the mechanism underlying the importance of TRIC-B in bone. Bone geometrical properties were severely impaired both at trabecular and cortical level and resembled those reported in transiliac biopsy samples for OI type XIV patients (17). Clusters of thicker collagen fibres were detected in cortical bone, revealing altered organization in cKO animals.

A fine-tuned intracellular Ca^{2+} level is necessary for OBs differentiation (25) and here we proved that the altered ionic homeostasis in cKO mice account for OBs alterations. In particular, we demonstrated an impaired SMAD signalling pathway caused mainly by a reduced activation of CaMKII-mediated signalling but also associated with reduced reservoir of TGF-β, a key cytokine for bone development and maintenance (39). It is well known that OBs have abundant TGF-β receptors, and that TGF-β1, upon binding to its receptor, induces phosphorylation of SMAD2/3, which can then form heterocomplexes with SMAD4 followed by translocation into the nucleus to upregulate osteogenesis-related genes (40, 41). The role of CaMKII signaling in bone is comparatively less understood. A few pivotal studies demonstrated that CaMKII is expressed in OBs, where it acts as a key regulator of OB differentiation (14, 42). Of relevance, *in vitro* inhibition of CaMKII in OB-like cells (MC4) reduced alkaline phosphatase activity and mineralization, as well as caused a strong decrease in alkaline phosphatase and osteocalcin gene expression. In an *in vivo* model, CaMKII antagonists decreased OB number and the bone volume/total volume ratio (14). Importantly, reduced alkaline phosphatase activity and mineralization, as well as decreased osteocalcin and *Osx* gene expression, were here found in TRIC-B cKO osteoblasts while a decreased BV/TV was found in cKO bone.

How the CaMKII defect is transduced to cause the bone defect is also poorly understood. In a human kidney fibroblast cell line, a link was established between CaMKII and SMAD2 nuclear localization and transcriptional function, independent of TGF-β, in the presence of a constitutively active CaMKII (43). In undifferentiated mesenchymal cells, activation of SMAD protein signaling through CaMKII by dentin phosphophoryn was shown to promote the expression of the osteogenic markers Runx2, Osterix, bone sialoprotein and osteocalcin (44). Similarly, in normal articular chondrocytes, targeted blockade of CaMKII with specific siRNAs decreased the levels of pSMADs, collagen type II, collagen type X and proteoglycans in the presence of TGF-β1, while CaMKII inhibitors caused a decrease of chondrogenic differentiation both in human foetal and pluripotent stem cells-derived chondrocytes (45). Furthermore, a direct interaction between SMADs and pCaMKII was found by immunoprecipitation studies in primary chondrocytes. In OBs it has been reported that CaMKII directly interacts with Osterix, the zinc-finger transcription factor required for OB differentiation and new bone formation, by increasing its protein level and enhancing its transcriptional activity (42).

Here, we proved for the first time that in OBs CaMKII controls SMAD-mediated signalling independently from TGF-β, revealing a novel Ca^{2} dependent mechanism for regulating

the activity of SMADs in bone. We demonstrated that, in control OBs, the inhibition of CaMKII by the calmodulin antagonist KN93 strongly reduces pSMAD3 level in the absence or presence of TGF-β, indicating a direct link between CaMKII and SMAD3 in OBs. In contrast, we found minimal effect on pSMAD3 level in cKO, indicating the CaMKII activity dependence on TRIC-B. Since the administration of TGF-β was not sufficient to revert the cell phenotype, we reason that the lower TGF-β reservoir in TRIC-B knock-out animals is secondary to the impairment of the CaMKII-mediated signalling and to the consequent delay in OB differentiation and reduced collagen in matrix.

Our study focused on the TRIC-B function in OBs. It should also be taken into account that the channel is ubiquitously expressed and its role in the other bone cells, as well as in different organs, should be investigated to fully dissect the patients' outcome. An altered osteoclast activity was found in the global TRIC-B KO, supporting the relevance of further investigations on this cell type (21).

In conclusion, our work links the bone phenotype associated with TRIC-B loss of function with the CaMKII signalling pathway in bone development and OB differentiation, adding a new piece of information on bone biology. This knowledge will help to refine strategies for the development of therapeutic approaches.

Methods

Animals

The animals used in the study were C57Bl/6Ngrey mice, generated by PolyGene and the FVB/NTg(*Runx2-Cre*) mice provided by Prof. Tuckermann (University of Ulm, Germany). Mice were maintained under standard experimental animal care protocol following the Italian Laws in the "Centro interdipartimentale di servizio per la gestione unificata delle attività di stabulazione e di radiobiologia - Polo Botta II" of the University of Pavia, Pavia (Italy).

Generation of *Tmem38b Runx2* conditional knock-out

A vector for the stable excision of exon 3 of the *Tmem38b* gene with a *loxP* system mediated by Cre-recombinase was generated. Three *loxP* sites were inserted flanking exon 3 of *Tmem38b* (Supplementary Fig. 1A). Additionally, different restriction sites were synthesized upstream, downstream and in between the *lox* sites, to allow insertion of different cassettes. For *in vitro* selection of targeted cells, we took advantage of an FRT flanked *neomycin* resistance gene cloned between the *lox*-sites using *BglII* upstream of exon 3 (Supplementary Fig. 1A). The targeting vector bearing the *Tmem38b* mutation was electroporated into 2×10^7 C57Bl/6N-based ES cells cultured with mitomycin C-inactivated mouse embryonic fibroblasts, in DMEM (Gibco) containing 20% fetal calf serum (Pansera ES, PAN), supplemented with leukemia inhibitory factor (ESLIF, PolyGene) and tissue culture factors to maintain pluripotent state ("2i": CT/CHIR 99201, and PD 0325910, Axon Medchem). After selection with 200 μg/mL neomycin (G418) for 8 days, embryonic stem (ES) cell clones were isolated and analyzed via PCR and Southern blot screening. Karyotyping was performed on positive ES cell clones in which correct homologous

recombination was occurred. For mouse generation, 3–4 positive ES cell clones were injected into grey C57Bl/6N derived blastocysts. These injections yielded 6 pups, three of which were high chimeric male. The resulting chimeras were bred to C57Bl/6Ngrey-based Flp-deleter female mice and yielded black (i.e. germ line) offspring, following a Mendelian rate. The resulting black offsprings were analyzed by PCR as detailed below. After the confirmation of the deletion of the *neomycin* cassette and of the presence of the *floxed* allele, *Tmem38b*$^{fl/fl}$ mice were mated to Tg(*Runx2-Cre*) mice, carrying the Cre recombinase under the Runt-related transcription factor 2 (Runx2) promoter, to generate the homozygous exon 3 bone specific conditional knock-out (*Runx2Cre;Tmem38b*$^{fl/fl}$) (Supplementary Fig. 1A). Exon 3 deletion was proved by PCR of genomic DNA of the target region and by sequence of the intronic LoxP site left upon Cre recombinase in the mutated alleles (Supplementary Fig. 1B, C, D). DNA sequencing confirmed the successful KO generation (Supplementary Fig. 2A). Four-week-old *Runx2Cre;Tmem38b*$^{fl/fl}$ mice and *Tmem38b*$^{fl/fl}$ littermate control mice were used for the analyses.

Tissue isolation

For genotyping, tail biopsy was performed in P28 animals. For confirmation of the osteoblast specific conditional gene inactivation and for phenotyping, mice were sacrificed at P28 by cervical dislocation following anesthesia and tissues were collected. DNA, RNA and protein were extracted from bone tissue cleaned from soft tissues and, from bone marrow that, after cutting the epiphysis, was flushed out with a 24-gauge needle syringe filled with ice-cold phosphate buffered saline (PBS). Bone was minced and decalcified in 14% EDTA pH 7.1 for 48 hours to obtain DNA; was minced in Trizol (Invitrogen) and stored at −80°C for RNA extraction; and stored at − 80°C until used for protein extraction.

Mice genotyping

The generated mice were analyzed by PCR for the presence of the recombinant locus using the primers G044.5F/G044.6R (5'-AATAGTAGGCGGAGTCTCGG-3' and 5'-TCTGGTGCCCTCTTCTTC-3', respectively) (PCR5/6) and the primers G044.9F/G044.8R (5'-GAGGAGATGCTGAAGAAC-3' and 5'-GGCGTAACACAACCAAAG-3', respectively) (PCR8/9, Supplementary Figure 1A, B, D, E). Homozygous exon 3 bone specific deletion was checked by PCR using primers G044.9F (5'-GAGGAGATGCTGAAGAAC-3') and G044.6R (5'-TCTG GTGCCCTCTTCTTC-3'). The PCR amplicon (Supplementary Figure 1C), present as expected in *Runx2Cre;Tmem38b*$^{fl/fl}$ bone and absent in *Tmem38b*$^{fl/fl}$, was then sequenced (Supplementary Figure 2A).

Murine calvarial and human osteoblast (OB) culture

Murine OBs were isolated from 2–4 days old control (*Tmem38b*$^{fl/fl}$) and mutant (*Runx2Cre;Tmem38b*$^{fl/fl}$) pups following a well-established protocol (46). For each experiment only cells at passage 1 were used plated at $1.5\times10^4/cm^2$, cultured in minimum essential medium eagle with α-modification (α-MEM) with 10% foetal bovine serum (FBS), antibiotics, and 50 μg/ml ascorbic acid (Sigma-Aldrich) and harvested after 5 days. For TGF-β treatment, cells were treated with 50 ng/mL TGF-β (Sino Biological, 80116-RNAH) for 1h. For CaMKII inhibition, cells were incubated with 1 μM KN-93 (Sigma Aldrich) for 1h. For mineralization studies, cells were cultured in α-MEM with 10% FBS,

antibiotics and supplemented with100 μg/ml ascorbic acid, and 10 mM β-glycerophosphate (Sigma-Aldrich) (osteogenic medium). Cells were treated with 1 ng/mL TGF-β every other day for one week and cultured for 21 days or every other day for 21 days. Harvest was performed at different time points, as detailed for each experiment.

Human OBs were isolated from bone chips of a 13 years old TMEM38B-null male OI patient showing a moderately severe phenotype (17, 22) and from healthy age-matched donor. Bone chips were digested in α-MEM (Gibco) with antibiotics and collagenase P (Roche) for 2 hours at 37 °C. After digestion, bone chips were cultured in α-MEM supplemented with antibiotics and 10% FBS (Gem Cell, Gemini Bio) at 37 °C, 8% CO_2 for couple of weeks until cells were expanded. For TGF-β signalling, control and patient pre-OB were seeded in 6-well plates. At sub-confluency, cells were serum starved for 1 hour, then treated with 5 ng/ml recombinant human TGF-β1 (7754-BH, R&D). Harvest was performed at different time points, as detailed in figure legend.

Gene expression analysis

Total RNA was extracted from bone, from OBs after 5 days of culture in growth media, and from OBs after 7, 14, 21, 28 days of culture in osteogenic medium and DNA integrity was checked on agarose gel. *Tmem38b, Osx, Alp, Bglap, Col1a1*and *Cdk1a* qRT-PCR were performed on the QuantStudio3 thermocycler (Thermofisher) using PowerUp Syber Green Master Mix (Applied Biosystems). *Gapdh* was used as normalizer. Primers sequences are available upon request. Relative expression was calculated using the ΔΔCt method. All reactions were performed in triplicate.

Protein lysates and western blot

Protein lysates were obtained from minced bones and from OBs using RIPA lysis buffer supplemented with protease inhibitors as previously described(47). Following protein quantitation using RC DC Protein Assay (BioRad), proteins were separated on 6% (collagen), 9% (pSMAD2 and SMAD2/3), 10% (TRIC-B, HSP47) or 15% (TGF-β) SDS-PAGE and transferred on PVDF membrane. The membranes were incubated o/n at 4°C with 1:1000 anti-TRIC-B (Invitrogen), anti-SMAD2/3 (Cell Signaling), anti-pSMAD2 (Abcam), anti-pSMAD3 (Abcam), anti-HSP47 (Santa Cruz) anti-collagen I (Abcam), anti-TGF-b (R&D System), anti-pCaMKII (Abcam) antibodies in TBS-T. ImageQuant LAS 4000 (GE Healthcare) and the ImageQuant LAS 4000 1.2 software were used for images acquisition. ImageQuant TL analysis software was employed for band intensity evaluation. At least biological triplicates were performed. For each gel, the expression of the mutant samples was expressed as fold difference compared to controls. Protein loading normalization was determined using anti-β-actin antibody (Santa Cruz Biotechnology) or total proteins staining by Swift™ Membrane Stain (G-Biosciences). For human cells, the following antibodies and dilutions were used: anti-pSMAD3 (phospho S423/S425) 1:1000 (Rockland) and anti-GAPDH 1 :1000 (Cell Signaling).

Growth curve evaluation and skeletal analyses

Mice growth curve was obtained by weighting the mice (n = 7 per group) once a week for 4 weeks. Results were analyzed based on gender and genotype. Skeletal characterization of

mice was performed by X-ray analyses (Faxitron) and using double staining with alcian blue and alizarin red. Mice (n = 7 per group) radiography were acquired, after anesthesia, using the Mx-20 multifocus digital radiography system (Faxitron Bioptics) set at 25 kV for 19 seconds, at 1.5X and 4X magnifications and visualized with the Kodak DirectView elite CR System K-Pacs software (Kodak) as previously described (48).

For alcian blue and alizarin red staining, mice (n = 4 per group) were sacrificed and processed as previously reported (49). Mice were imaged by Leica M165 FC stereomicroscope connected to a Leica DFC425 digital camera (Leica Microsystems, Italy).

Bone structural properties by μCT

μCT analyses of tibia from *Runx2Cre;Tmem38b*$^{fl/fl}$ and *Tmem38b*$^{fl/fl}$ littermate control mice were performed at P28 (n = 7 per genotype for each gender). Bones were scanned at a nominal image resolution of 11 μm by means of a SkyScan μCT 1276 scanner (Skyscan, Kontich, Belgium) at 55 kV and 200 μA, using a 0.25 mm aluminum filter. Images were captured every 0.4° through 180° of rotation with a 2×2 camera pixel binning. The reconstruction was carried out with the SkyScan NRecon software using the InstaRecon reconstruction engine, ring artifact reduction and beam hardening correction. Image analysis was performed by means of the CT Analyser software (CTAn). The reference slice was imposed at the level of the growth plate. Trabecular and cortical regions were set 70 and 400 slices below the reference slice and normalized to tibia length. For bone segmentation a semiautomatic approach was used, based on thresholding. The thresholding was standardized with the CTAn software across all bone samples using global threshold (70–255) for trabecular bone 3D analyses. A global threshold (95–255) was used for the cortical bone 3D analyses. The mean BMD of the segmented regions was calculated by resorting to a calibration based on a linear extrapolation against mean attenuation coefficients from selected regions of a 2 mm phantom rod pair containing 0.25 and 0.75 g/cm^{-3} CaHA (Skyscan). The ratio between bone volume to total volume (BV/TV, %), the bone surface (BS, mm^2), the intersection surface (IS, mm^2) and trabecular thickness (Tb Th, mm) were assessed for the trabecular bone. Bone volume (BV, mm^3), bone surface to bone volume ratio (BS/BV, mm^{-1}), the intersection surface (IS, mm^2) and cortical thickness (Ct Th, mm) were assessed for the cortical bone.

Bone histology

Tibiae at P30 were dissected, cleaned from surrounding connective tissue and fixed in 4% paraformaldehyde (PFA) in PBS for 24 h. Bones were then decalcified in 14% EDTA pH 7.1 for 21 days and embedded in paraffin following standard procedures. Longitudinal tibia sections (7 μm) were cut using a RM2265 microtome (Leica Microsystems srl), mounted on Superfrost Plus slides (Menzel-Glaser, VWR) and stained with Alcian Blue Hematoxylin and Orange G/Eosin Counterstain or Sirius red staining. Images were acquired using a DFC480 digital camera (Leica Microsystems srl) connected to a light microscope (DM5500B, Leica, Microsystems srl). Sirius red-stained sections were analyzed under polarized light, and images were acquired by Leica DM2500 equipped with L ICT/P polarizer and a digital color camera LEICA DFC295 (Leica).

Mineralization assays and alkaline phosphatase activity

To evaluate mineralization, OBs cultured for day 21 in osteogenic medium were stained by alizarin red and ALP activity was measured using the Abnova alkaline phosphatase kit as described in (50).

Transmission electron microscopy analysis

Transmission electron microscopy analysis was performed on trypsinized and pelleted OBs as previously described (47).

Thioflavin T labelling

Thioflavin (ThT, Sigma-Aldrich) labelling was performed on OBs from six independent preparations plated on sterile glass coverslips (Marienfeld) as previously described (47). Images acquisition was obtained by SP8-Leica confocal microscope (Leica) and the Leica software LAS4.5 was used to evaluate fluorescence signal per cell. A total of 41–45 cells for each OB preparation was evaluated.

Cell proliferation

OBs were plated at 5×10^3 cells/well in 96 well/plate in complete growing medium and cell proliferation was evaluated by Cell Titer 96 AQueous Cell proliferation Assay (Promega). Technical triplicates were performed.

Protein synthesis

OBs were labelled with 5 mCi/ml [35S] EXPRESS35S Protein Labeling Mix (PerkinElmer) in α-MEM without L-methionine, L-cystine, and L-glutamine for 1 h at 37 °C.
The experiment was performed on three independent OB preparations. Upon protein precipitation, the radioactivity (counts for minute, CPM) of the samples was quantified using a liquid scintillation analyzer (TRI-CARB 2300 TR) (47).

Collagen quantification in OBs' matrix and media

Cells were cultured for 21 days in osteogenic medium to allow matrix deposition. Media was collected and matrix was decellularized. Collagen was extracted and quantified by Sircol™ Soluble Collagen Assay (Biocolor), according to the manufacturer's protocol, on three independent OBs preparations.

Collagen analysis

Collagen was extracted by pepsin digestion and salt precipitation from decalcified bone (n=3 for each genotype), run on 6% urea-SDS gel in non-reducing condition and stained by Coomassie blue as previously reported (51).

Calcium measurements

The recombinant Ca^{2+}-sensitive photoprotein aequorin specifically targeted to the mitochondrial matrix (52) was employed to measure Ca^{2+} uptake by the mitochondria which reflects the Ca^{2+} microdomains generated at the mouth of the InsP3 channels upon their opening (53). For cytosolic and mitochondrial calcium measurements using the aequorin

method, OBs were plated into a 96-well plate at 50–60% of confluence and transduced for 48h in their culture medium with adenovirus expressing cytosolic or mitochondrial aequorin (cytAEQ or mtAEQ). 48h post adenoviral transduction cells were incubated (1 hr, 37°C) with the prosthetic group coelenterazine (5 μM, 1 h at 37°C, Santa Cruz Biotechnology) in $CaCl_2$-containing Krebs-Ringer buffer (KRB - $CaCl_2$, 125 mM NaCl, 1 mM Na_3PO_4, 1 mM $MgSO_4$, 1 mM $CaCl_2$, 5.5 mM glucose, 5 mM KCl, 20 mM HEPES, pH 7.4). After aequorin reconstitution, cells were placed in 70 μl of KRB-$CaCl_2$ and cytosolic or mitochondrial Ca^{2+} transients were evoked by applying 100 μM ATP (Amersham Biosciences) in KRB. Cytosolic and mitochondrial calcium measurements were carried out using a PerkinElmer EnVision plate reader equipped with two injector units. Output data were analyzed and calibrated with a custom-made macro-enabled Excel workbook.

pSMAD3 immunofluorescence

2×10^4 OBs were plated on glass coverslips in 24 well plate. The next day cells were treated for 24 h with 1 ng/mL TGF-β. Cells were fixed with 10% neutral buffered formalin for 30 min at RTand blocked 1 h in 1% BSA in PBS containing 0.3% TritonX100. pSMAD3 primary antibody (Abcam) was used at 1:500 dilution in 1% BSA, 0.3% TritonX100 in PBS and the incubation was carried out o/n at 4°C. Cells were incubated with secondary antibody (AlexaFluor 488 conjugated F(ab') fragment anti-rabbit IgG, Immunological Sciences) 1:2000 in 1% BSA, 0.3% TritonX100 in PBS for 2 h at RT. Nuclei were stained with DAPI and images were acquired by confocal microscope TCS SP8 (Leica). The total area of punctate signal per cell and of punctate signal per nucleus were measured by the Leica software LAS 4.5.

Statistics

For the *in vivo* studies, 7 animals for each genotype and gender were used. For the *in vitro* studies, at least biological triplicates for each genotype were performed. The sample size is specified in the method section. Quantitative variables were expressed as mean ± standard deviation (SD). One-way repeated measures ANOVA was applied to evaluate genotype effect followed by post-hoc tests with the Bonferroni's correction. A p value <0.05 was considered significant.

Study approval

All animal studies were approved by the Italian Animal Research Council under the Protocol N 8/2019-PR approved on Oct 8th 2019. The human study was approved by the NICHD IRB (Protocol #04-CH-0077). Cells from Proband were obtained as part of the diagnostic process. Written, informed consent was obtained from all subjects or their respective guardians.

Supplementary Material

Refer to Web version on PubMed Central for supplementary material.

Acknowledgements

We thank Dr. Patrizia Vaghi and Dr. Amanda Oldani, Centro Grandi Strumenti, University of Pavia, Italy, for the confocal analysis support; the animal facility “Centro di servizio per la gestione unificata delle attività di stabulazione e di radiobiologia” of the University of Pavia, Pavia, Italy to host the animals; the OPBA of the University of Pavia for support with animal protocol.

Funding

This work was supported by Italian Ministry of Education, University and Research (MIUR) [Dipartimenti di Eccellenza (2018–2022)] to AF; by the FP7 Ideas: European Research Council “Sybil” project [grant no. 602300] to AF; by Regione Lombardia, “regional law n° 9/2020, resolution n° 3776/2020” to AF; by Fondazione Telethon grant no. GMR22T1024 to RB.

References

1. Yazawa M, Ferrante C, Feng J, Mio K, Ogura T, Zhang M, et al. TRIC channels are essential for Ca2+ handling in intracellular stores. Nature. 2007;448(7149):78–82. [PubMed: 17611541]
2. Yamazaki D, Komazaki S, Nakanishi H, Mishima A, Nishi M, Yazawa M, et al. Essential role of the TRIC-B channel in Ca2+ handling of alveolar epithelial cells and in perinatal lung maturation. Development. 2009;136(14):2355–61. [PubMed: 19515693]
3. Hu Z, and Gulyaeva O. TRIC-B: an under-explored druggable ion channel. Nat Rev Drug Discov. 2019;18(9):657. [PubMed: 31477859]
4. O’Brien F, Eberhardt D, Witschas K, El-Ajouz S, Iida T, Nishi M, et al. Enhanced activity of multiple TRIC-B channels: an endoplasmic reticulum/sarcoplasmic reticulum mechanism to boost counterion currents. J Physiol. 2019;597(10):2691–705. [PubMed: 30907436]
5. Cremer T, Neefjes J, and Berlin I. The journey of Ca^{2+} through the cell-pulsing through the network of ER membrane contact sites. J Cell Sci. 2020;133(24).
6. Patergnani S, Danese A, Bouhamida E, Aguiari G, Previati M, Pinton P, et al. Various Aspects of Calcium Signaling in the Regulation of Apoptosis, Autophagy, Cell Proliferation, and Cancer. Int J Mol Sci. 2020;21(21).
7. Berridge MJ. The Inositol Trisphosphate/Calcium Signaling Pathway in Health and Disease. Physiol Rev. 2016;96(4):1261–96. [PubMed: 27512009]
8. Gaspers LD, Bartlett PJ, Politi A, Burnett P, Metzger W, Johnston J, et al. Hormone-induced calcium oscillations depend on cross-coupling with inositol 1,4,5-trisphosphate oscillations. Cell Rep. 2014;9(4):1209–18. [PubMed: 25456123]
9. Filadi R, and Pozzan T. Generation and functions of second messengers microdomains. Cell Calcium. 2015;58(4):405–14. [PubMed: 25861743]
10. Teitelbaum SL. Bone resorption by osteoclasts. Science. 2000;289(5484):1504–8. [PubMed: 10968780]
11. Purroy J, and Spurr NK. Molecular genetics of calcium sensing in bone cells. Hum Mol Genet. 2002;11(20):2377–84. [PubMed: 12351573]
12. Theman TA, and Collins MT. The role of the calcium-sensing receptor in bone biology and pathophysiology. Curr Pharm Biotechnol. 2009;10(3):289–301. [PubMed: 19355939]
13. Khoshniat S, Bourgine A, Julien M, Petit M, Pilet P, Rouillon T, et al. Phosphate-dependent stimulation of MGP and OPN expression in osteoblasts via the ERK1/2 pathway is modulated by calcium. Bone. 2011;48(4):894–902. [PubMed: 21147284]
14. Zayzafoon M, Fulzele K, and McDonald JM. Calmodulin and calmodulin-dependent kinase IIalpha regulate osteoblast differentiation by controlling c-fos expression. J Biol Chem. 2005;280(8):7049–59. [PubMed: 15590632]
15. Mandal CC, Das F, Ganapathy S, Harris SE, Choudhury GG, and Ghosh-Choudhury N. Bone Morphogenetic Protein-2 (BMP-2) Activates NFATc1 Transcription Factor via an Autoregulatory Loop Involving Smad/Akt/Ca2+ Signaling. J Biol Chem. 2016;291(3):1148–61. [PubMed: 26472929]

16. Nesti LJ, Caterson EJ, Li WJ, Chang R, McCann TD, Hoek JB, et al. TGF-beta1 calcium signaling in osteoblasts. J Cell Biochem. 2007;101(2):348–59. [PubMed: 17211850]
17. Webb EA, Balasubramanian M, Fratzl-Zelman N, Cabral WA, Titheradge H, Alsaedi A, et al. Phenotypic Spectrum in Osteogenesis Imperfecta Due to Mutations in TMEM38B: Unraveling a Complex Cellular Defect. J Clin Endocrinol Metab. 2017;102(6):2019–28. [PubMed: 28323974]
18. Marini JC, Forlino A, Cabral WA, Barnes AM, San Antonio JD, Milgrom S, et al. Consortium for osteogenesis imperfecta mutations in the helical domain of type I collagen: regions rich in lethal mutations align with collagen binding sites for integrins and proteoglycans. Hum Mutat. 2007;28(3):209–21. [PubMed: 17078022]
19. Besio R, Chow CW, Tonelli F, Marini JC, and Forlino A. Bone biology: insights from osteogenesis imperfecta and related rare fragility syndromes. FEBS J. 2019;286(15):3033–56. [PubMed: 31220415]
20. Jovanovic M, Guterman-Ram G, and Marini JC. Osteogenesis Imperfecta: Mechanisms and Signaling Pathways Connecting Classical and Rare OI Types. Endocr Rev. 2022;43(1):61–90. [PubMed: 34007986]
21. Zhao C, Ichimura A, Qian N, Iida T, Yamazaki D, Noma N, et al. Mice lacking the intracellular cation channel TRIC-B have compromised collagen production and impaired bone mineralization. Sci Signal. 2016;9(428):ra49.
22. Cabral WA, Ishikawa M, Garten M, Makareeva EN, Sargent BM, Weis M, et al. Absence of the ER Cation Channel TMEM38B/TRIC-B Disrupts Intracellular Calcium Homeostasis and Dysregulates Collagen Synthesis in Recessive Osteogenesis Imperfecta. PLoS Genet. 2016;12(7):e1006156.
23. Beriault DR, and Werstuck GH. Detection and quantification of endoplasmic reticulum stress in living cells using the fluorescent compound, Thioflavin T. Biochim Biophys Acta. 2013;1833(10):2293–301. [PubMed: 23747341]
24. Ishida Y, and Nagata K. Hsp47 as a collagen-specific molecular chaperone. Methods Enzymol. 2011;499:167–82. [PubMed: 21683254]
25. Zayzafoon M. Calcium/calmodulin signaling controls osteoblast growth and differentiation. J Cell Biochem. 2006;97(1):56–70. [PubMed: 16229015]
26. Hanson PI, Kapiloff MS, Lou LL, Rosenfeld MG, and Schulman H. Expression of a multifunctional Ca2+/calmodulin-dependent protein kinase and mutational analysis of its autoregulation. Neuron. 1989;3(1):59–70. [PubMed: 2619995]
27. Hudmon A, and Schulman H. Neuronal CA2+/calmodulin-dependent protein kinase II: the role of structure and autoregulation in cellular function. Annu Rev Biochem. 2002;71:473–510. [PubMed: 12045104]
28. Wu X, and McMurray CT. Calmodulin kinase II attenuation of gene transcription by preventing cAMP response element-binding protein (CREB) dimerization and binding of the CREB-binding protein. J Biol Chem. 2001;276(3):1735–41. [PubMed: 11013247]
29. Lisman J, Yasuda R, and Raghavachari S. Mechanisms of CaMKII action in long-term potentiation. Nat Rev Neurosci. 2012;13(3):169–82. [PubMed: 22334212]
30. Ojuka EO, Goyaram V, and Smith JA. The role of CaMKII in regulating GLUT4 expression in skeletal muscle. Am J Physiol Endocrinol Metab. 2012;303(3):E322–31. [PubMed: 22496345]
31. De Koninck P, and Schulman H. Sensitivity of CaM kinase II to the frequency of Ca2+ oscillations. Science. 1998;279(5348):227–30. [PubMed: 9422695]
32. Leoni L, Tonelli F, Besio R, Gioia R, Moccia F, Rossi A, et al. Knocking out TMEM38B in human foetal osteoblasts hFOB 1.19 by CRISPR/Cas9: A model for recessive OI type XIV. PLoS One. 2021;16(9):e0257254.
33. Tonelli F, Leoni L, Daponte V, Gioia R, Cotti S, Fiedler IAK, et al. Zebrafish Tric-b is required for skeletal development and bone cells differentiation. Front Endocrinol (Lausanne). 2023;14:1002914.
34. Shaheen R, Alazami AM, Alshammari MJ, Faqeih E, Alhashmi N, Mousa N, et al. Study of autosomal recessive osteogenesis imperfecta in Arabia reveals a novel locus defined by TMEM38B mutation. J Med Genet. 2012;49(10):630–5. [PubMed: 23054245]

35. Volodarsky M, Markus B, Cohen I, Staretz-Chacham O, Flusser H, Landau D, et al. A deletion mutation in TMEM38B associated with autosomal recessive osteogenesis imperfecta. Hum Mutat. 2013;34(4):582–6. [PubMed: 23316006]
36. Caparros-Martin JA, Aglan MS, Temtamy S, Otaify GA, Valencia M, Nevado J, et al. Molecular spectrum and differential diagnosis in patients referred with sporadic or autosomal recessive osteogenesis imperfecta. Mol Genet Genomic Med. 2017;5(1):28–39. [PubMed: 28116328]
37. Rubinato E, Morgan A, D'Eustacchio A, Pecile V, Gortani G, Gasparini P, et al. A novel deletion mutation involving TMEM38B in a patient with autosomal recessive osteogenesis imperfecta. Gene. 2014;545(2):290–2. [PubMed: 24835313]
38. Lv F, Xu XJ, Wang JY, Liu Y, Asan Wang JW, et al. Two novel mutations in TMEM38B result in rare autosomal recessive osteogenesis imperfecta. J Hum Genet. 2016;61(6):539–45. [PubMed: 26911354]
39. Geiser AG, Zeng QQ, Sato M, Helvering LM, Hirano T, and Turner CH. Decreased bone mass and bone elasticity in mice lacking the transforming growth factor-beta1 gene. Bone. 1998;23(2):87–93. [PubMed: 9701466]
40. Harris SE, Bonewald LF, Harris MA, Sabatini M, Dallas S, Feng JQ, et al. Effects of transforming growth factor beta on bone nodule formation and expression of bone morphogenetic protein 2, osteocalcin, osteopontin, alkaline phosphatase, and type I collagen mRNA in long-term cultures of fetal rat calvarial osteoblasts. J Bone Miner Res. 1994;9(6):855–63. [PubMed: 8079661]
41. Dallas SL, Sivakumar P, Jones CJ, Chen Q, Peters DM, Mosher DF, et al. Fibronectin regulates latent transforming growth factor-beta (TGF beta) by controlling matrix assembly of latent TGF beta-binding protein-1. J Biol Chem. 2005;280(19):18871–80. [PubMed: 15677465]
42. Choi YH, Choi JH, Oh JW, and Lee KY. Calmodulin-dependent kinase II regulates osteoblast differentiation through regulation of Osterix. Biochem Biophys Res Commun. 2013;432(2):248–55. [PubMed: 23402759]
43. Wicks SJ, Lui S, Abdel-Wahab N, Mason RM, and Chantry A. Inactivation of smad-transforming growth factor beta signaling by Ca(2+)-calmodulin-dependent protein kinase II. Mol Cell Biol. 2000;20(21):8103–11. [PubMed: 11027280]
44. Eapen A, Kulkarni R, Ravindran S, Ramachandran A, Sundivakkam P, Tiruppathi C, et al. Dentin phosphophoryn activates Smad protein signaling through Ca2+-calmodulin-dependent protein kinase II in undifferentiated mesenchymal cells. J Biol Chem. 2013;288(12):8585–95. [PubMed: 23362283]
45. Saitta B, Elphingstone J, Limfat S, Shkhyan R, and Evseenko D. CaMKII inhibition in human primary and pluripotent stem cell-derived chondrocytes modulates effects of TGFβ and BMP through SMAD signaling. Osteoarthritis Cartilage. 2019;27(1):158–71. [PubMed: 30205161]
46. Bianchi L, Gagliardi A, Maruelli S, Besio R, Landi C, Gioia R, et al. Altered cytoskeletal organization characterized lethal but not surviving Brtl+/− mice: insight on phenotypic variability in osteogenesis imperfecta. Hum Mol Genet. 2015;24(21):6118–33. [PubMed: 26264579]
47. Garibaldi N, Contento BM, Babini G, Morini J, Siciliani S, Biggiogera M, et al. Targeting cellular stress in vitro improves osteoblast homeostasis, matrix collagen content and mineralization in two murine models of osteogenesis imperfecta. Matrix Biol. 2021;98:1–20. [PubMed: 33798677]
48. Paganini C, Gramegna Tota C, Monti L, Monti I, Maurizi A, Capulli M, et al. Improvement of the skeletal phenotype in a mouse model of diastrophic dysplasia after postnatal treatment with N-acetylcysteine. Biochem Pharmacol. 2021;185:114452.
49. Forlino A, Porter FD, Lee EJ, Westphal H, and Marini JC. Use of the Cre/lox recombination system to develop a non-lethal knock-in murine model for osteogenesis imperfecta with an alpha1(I) G349C substitution. Variability in phenotype in BrtlIV mice. J Biol Chem. 1999;274(53):37923–31.
50. Gregory CA, Gunn WG, Peister A, and Prockop DJ. An Alizarin red-based assay of mineralization by adherent cells in culture: comparison with cetylpyridinium chloride extraction. Anal Biochem. 2004;329(1):77–84. [PubMed: 15136169]
51. Maruelli S, Besio R, Rousseau J, Garibaldi N, Amiaud J, Brulin B, et al. Osteoblasts mineralization and collagen matrix are conserved upon specific *Col1a2* silencing. Matrix Biol Plus. 2020;6–7:100028.

52. Rizzuto R, Simpson AW, Brini M, and Pozzan T. Rapid changes of mitochondrial Ca2+ revealed by specifically targeted recombinant aequorin. Nature. 1992;358(6384):325–7. [PubMed: 1322496]

53. Rizzuto R, Brini M, Murgia M, and Pozzan T. Microdomains with high Ca2+ close to IP3-sensitive channels that are sensed by neighboring mitochondria. Science. 1993;262(5134):744–7. [PubMed: 8235595]

Highlights

- Lack of TRIC-B in osteoblasts strongly impairs skeleton growth and structure, leading to bone fractures.
- In absence of TRIC-B, the impaired Ca^{2+} flux from endoplasmic reticulum to cytosol is associated to delayed osteoblast differentiation and decreased collagen synthesis that cause reduced collagen incorporation in the extracellular matrix and poor mineralization.
- An impaired SMAD signalling in mutant mice and in OI patient osteoblasts explains the osteoblast malfunction.
- The reduced SMAD phosphorylation and nuclear translocation are mainly caused by alteration in Ca^{2+} calmodulin kinase II (CaMKII)-mediated signalling.

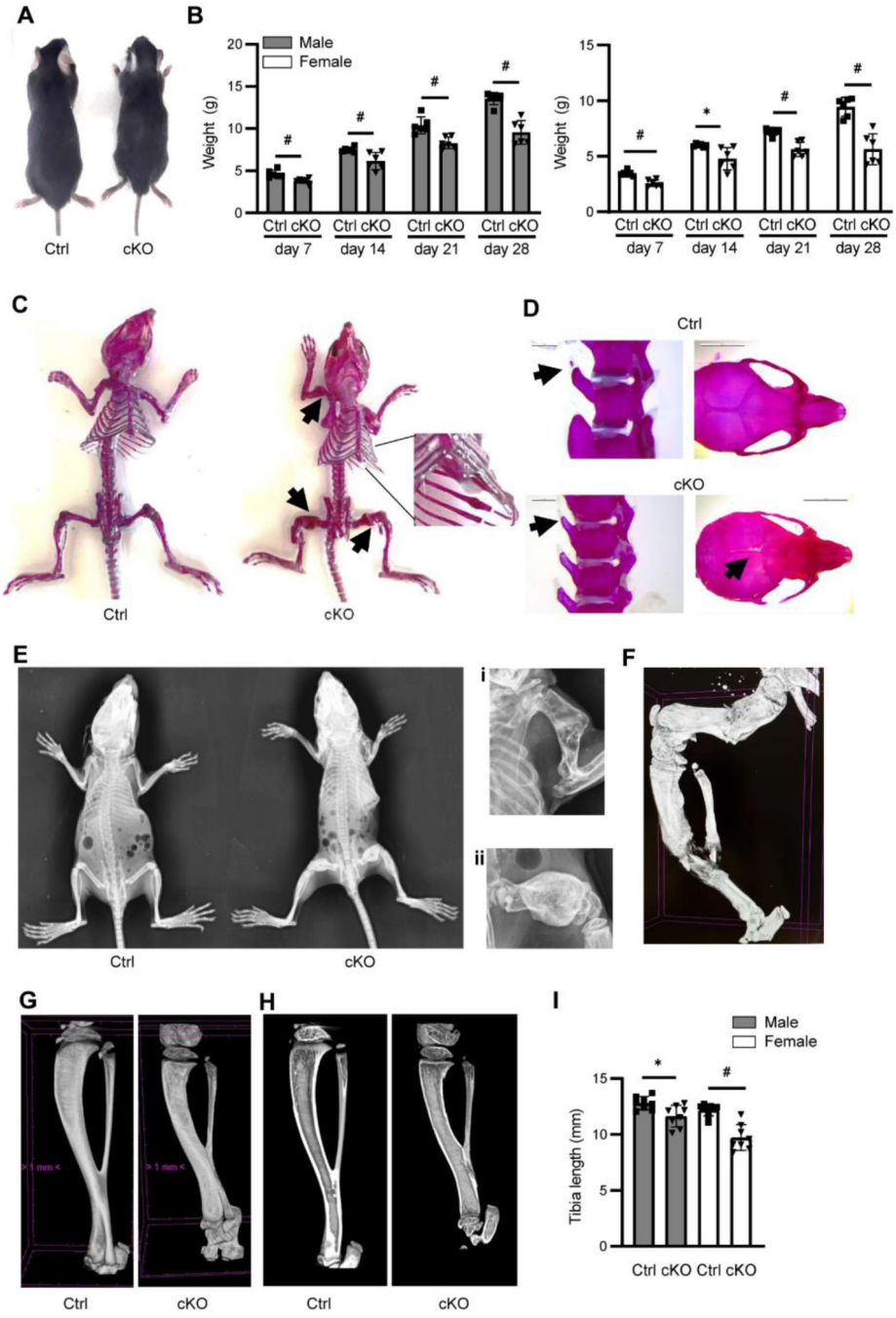

Figure 1: Bone phenotype in the TRIC-B OB conditional knock-out mice.

(**A**) Body size is reduced in *Tmem38b* osteoblast conditional knock-out (*Runx2Cre;Tmem38b*$^{fl/fl}$; cKO) compared to control mice (*Tmem38b*$^{fl/fl}$; Ctrl). (**B**) Growth curve analysis was performed from 1 to 4 weeks after birth. The analyses showed a growth delay in mutant mice in both genders. (**C**) Alcian blue and alizarin red skeletal staining performed on P28 animals revealed several calli (black arrows) in cKO bones. Calli in mutant ribs are shown in 4X magnification. (**D**) Magnification of mice vertebrae and skull proved a delay in cKO ossification (black arrows) (4X). (**E**) X-ray skeletal analysis revealed

the presence of calli and bone deformations in cKO mice at P28. (i) 4X magnification of mutant humerus with callus; (ii) 4X magnification of mutant femur with callus. (**F**) 3D micro CT reconstruction of femur and tibia from cKO mice with severe bone deformations and calli. (**G**) 3D tibia reconstruction and longitudinal section (**H**) of bones used for the structural analyses. (**I**) Tibia length was significantly shorter in cKO mice in both genders. * $p<0.05$; #$p<0.005$.

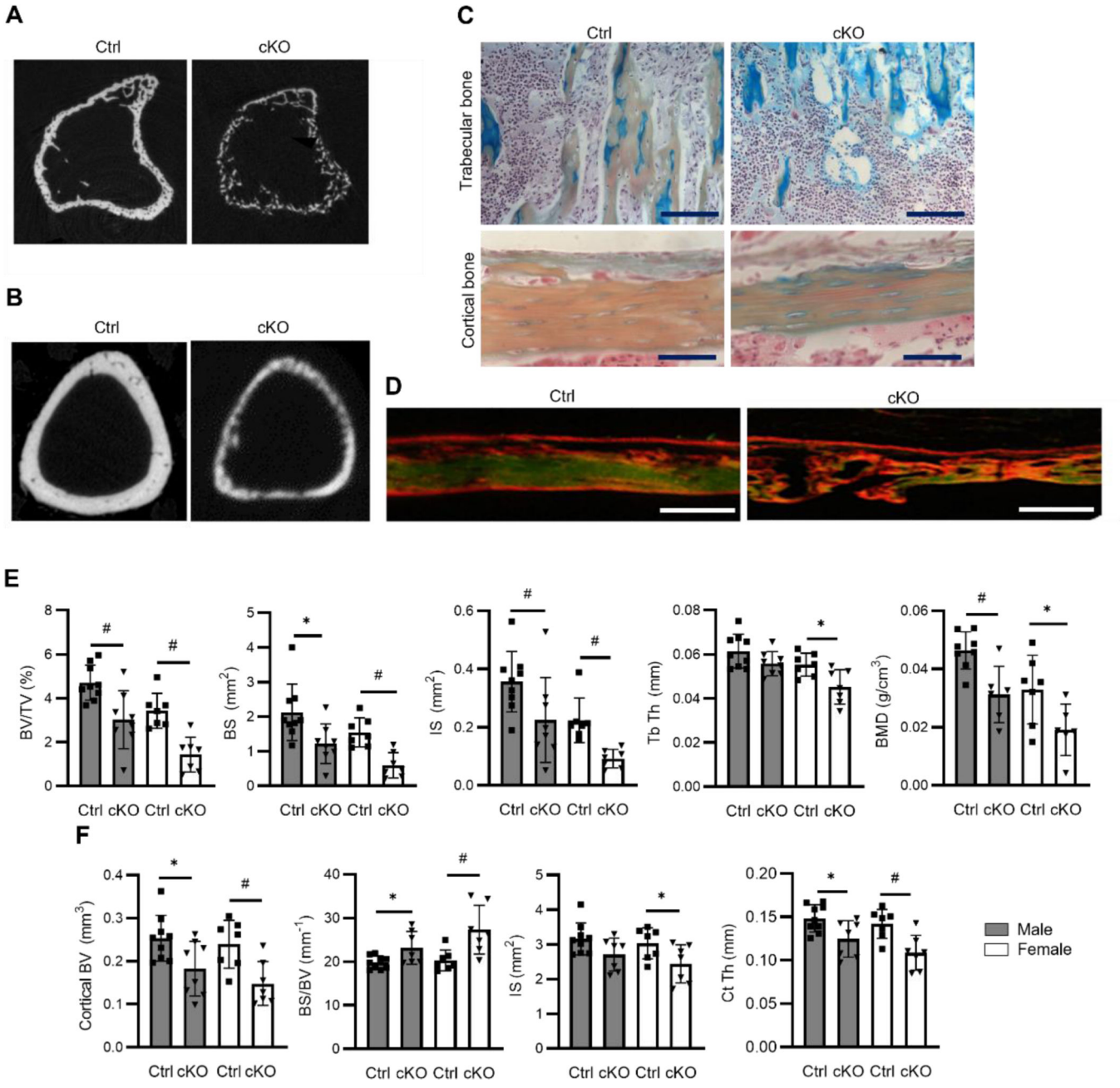

Figure 2: Altered trabecular and cortical bone properties in TRIC-B OB conditional knock-out mice.

Cross sectional tomographic images of (**A**) the trabecular and (**B**) the cortical bone. (**C**) Alcian Blue Haematoxylin staining of tibial distal metaphysis confirmed the impairment in trabecular and cortical compartments in cKO animals. Scale bar: 200 nm. (**D**) Picro-sirius red staining of tibial cortical bone at distal metaphysis revealed ticker collagen fibrils in cKO animals. Scale bar: 250 nm. (**E**) Trabecular and (**F**) cortical bone parameters of cKO and control male and female mice at P28. At the trabecular level, bone volume/total volume (BV/TV), bone surface (BS), intersection surface (IS), trabecular thickness (Tb Th) and bone mineral density (BMD) were significantly reduced in cKO mice. Similarly, in the

cortical compartment, BV, IS, and cortical thickness (Ct Th) were significantly reduced in cKO mice. By contrast, BS/BV was higher in cKO mice. * $p<0.05$; #$p<0.005$.

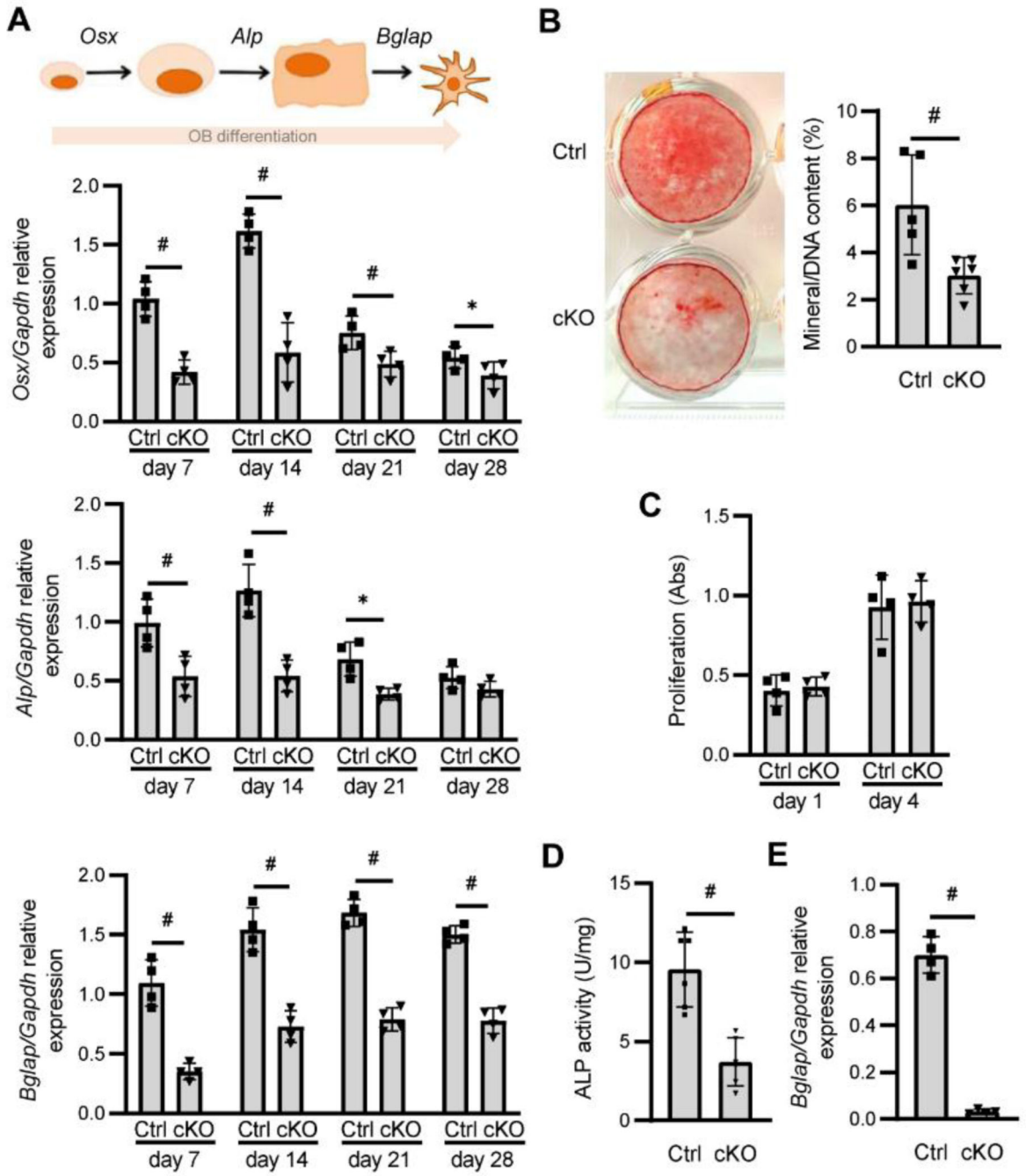

Figure 3: Impaired osteoblasts differentiation in TRIC-B OB conditional knock-out mice.

(**A**) Real time qPCR analyses of *Osx, Alp* and *Bglap* revealed a reduced expression in cKO calvaria OBs at day 7, 14, 21 and 28 of culture in osteogenic medium. (**B**) Alizarin red staining of primary OBs cultured in osteogenic medium. OBs mineral content was quantified. A decreased mineral staining was evident in mutant cells. (**C**) MTT assay revealed no difference in OBs proliferation between cKOs and controls. (**D**) ALP activity in osteogenic medium was evaluated by enzymatic assay. A significant reduction of ALP

activity was detected in mutant cells. (**E**) qPCR analyses of femur RNA confirmed the *Bglap* expression impairment in cKOs compared to controls. * $p<0.05$; #$p<0.005$.

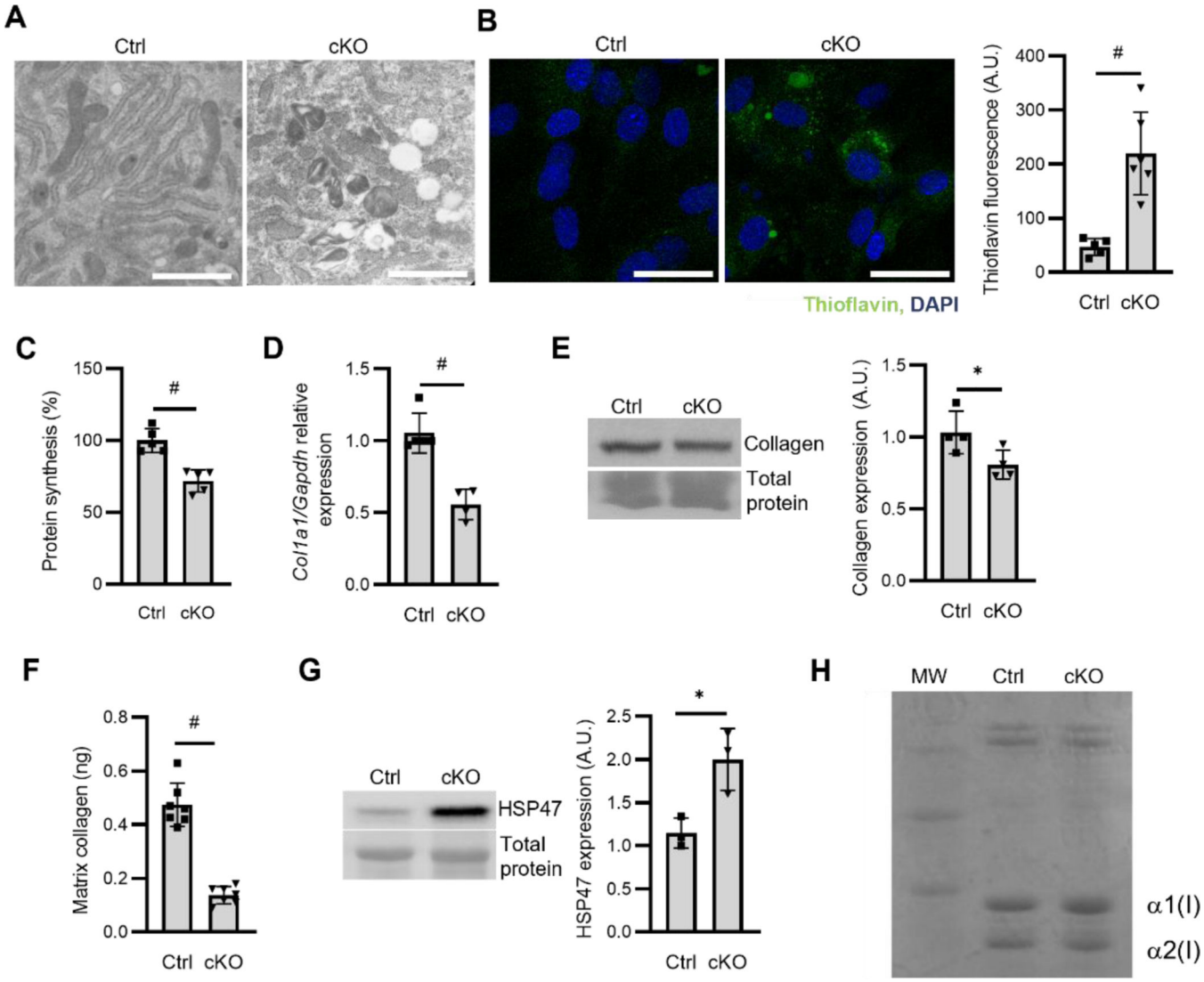

Figure 4: Decreased collagen synthesis and collagen incorporation into the matrix in TRIC-B cKO OBs.

(**A**) Transmission electron microscopy representative images of calvarial OBs. The analyses revealed ER enlargement and large vacuoles in all the mutant cells analyzed (n=18). Scale bar: 0.3 μm. (**B**) ER proteostasis was evaluated by thioflavin T (ThT) immunofluorescence. Representative images and ThT quantification are shown. ThT fluorescence was increased in mutant cells compared to control, highlighting the intracellular accumulation of misfolded proteins. Scale bar: 20 μm. (**C**) The quantification of proteins synthetized by OBs, evaluated following incorporation with ^{35}S-methionine and ^{35}S-cystine, showed a reduced protein amount in mutant cells. (**D**) Real time qPCR analyses of *Col1a1* revealed a reduced collagen expression in cKO OBs. (**E**) Cellular collagen protein level was reduced. (**F**) The amount of collagen incorporated into the extracellular matrix was evaluated in mutated and control OBs grown in osteogenic media for 7 days. Collagen content was reduced in mutant decellularized matrix. (**G**) Western blot analyses of HSP47 showed a strong upregulation in the mutant. (**H**) Collagen post translational modifications were assessed by SDS-Urea-

PAGE. Collagen type I from cKO mice bone revealed a faster migration of α(I) bands respect to control, supporting reduced hydroxylation and glycosylation. MW: molecular weight markers. * $p<0.05$; #$p<0.005$.

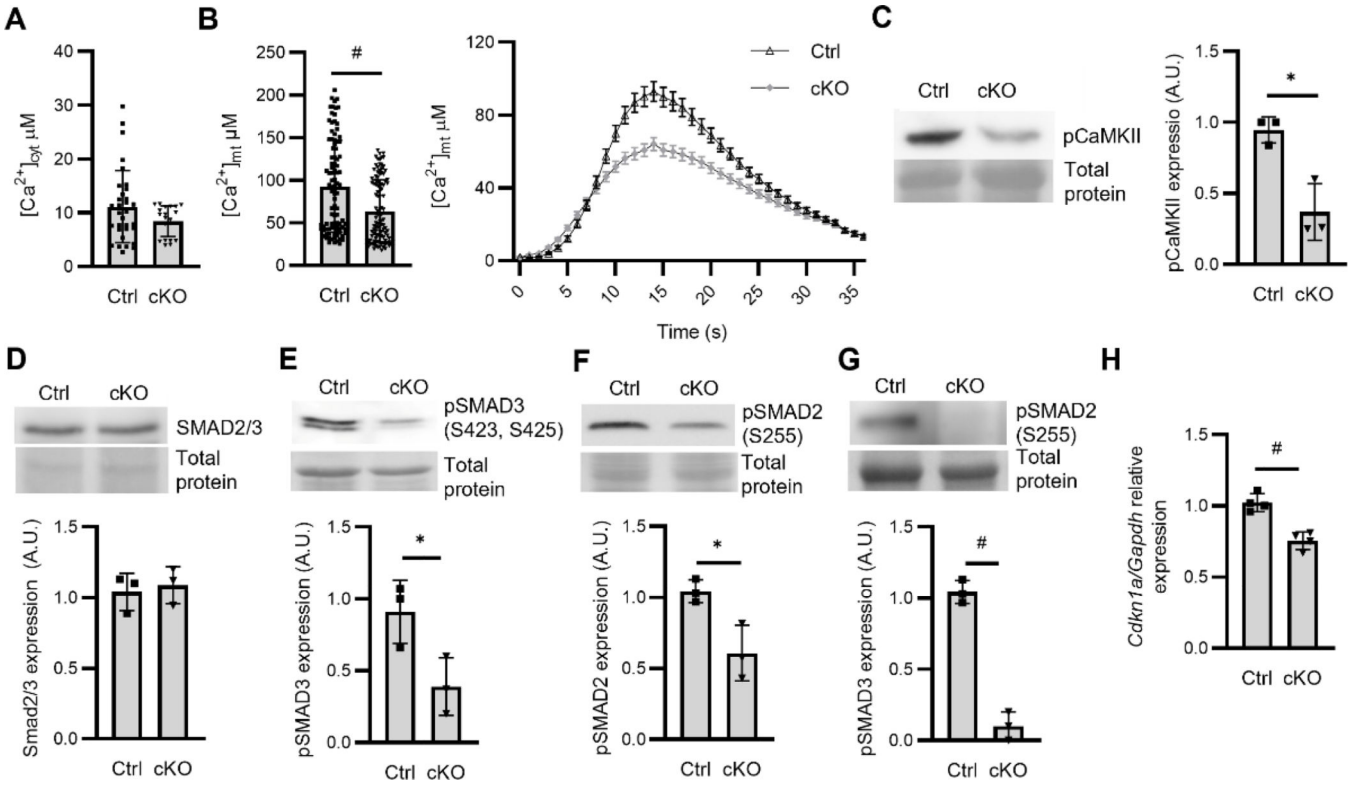

Figure 5: TRIC-B deficiency impairs Ca^{2+} calmodulin kinase II phosphorylation and SMAD signalling pathway.

Measurement of calcium transients by cytosolic (**A**) or mitochondrial (**B**) aequorin in OBs extracted from femur. Cells were stimulated with extracellular ATP, an inositol trisphosphate receptor ($InsP_3$) agonist, to induce Ca^{2+} release from the intracellular stores. The peak amplitude of cytosolic calcium ($[Ca^{2+}]_{cit}$) transients was unchanged in mutant versus control cells. A decreased calcium transient was instead found in mitochondria ($[Ca^{2+}]_{mit}$) from the cKO model (#p<0.0001). (**C**) Western blot analyses of CaMKII autophosphorylation at threonine 286. A decreased phosphorylation was found in cKO OBs. (**D**) Western blot analysis showed normal levels of SMAD2/3 in cKO OBs while decreased pSMAD3 (**E**) and pSMAD2 (**F**) levels were found. (**G**) Significantly reduced pSMAD2 level was confirmed in bone from *Runx2Cre;Tmem38b*$^{fl/fl}$ animals. Total protein was used to normalize protein expression. (**H**) Real time qPCR analyses of *Cdkn1*, a TGF-β target gene, revealed a reduced expression in cKO OBs. * p<0.05; #p<0.005.

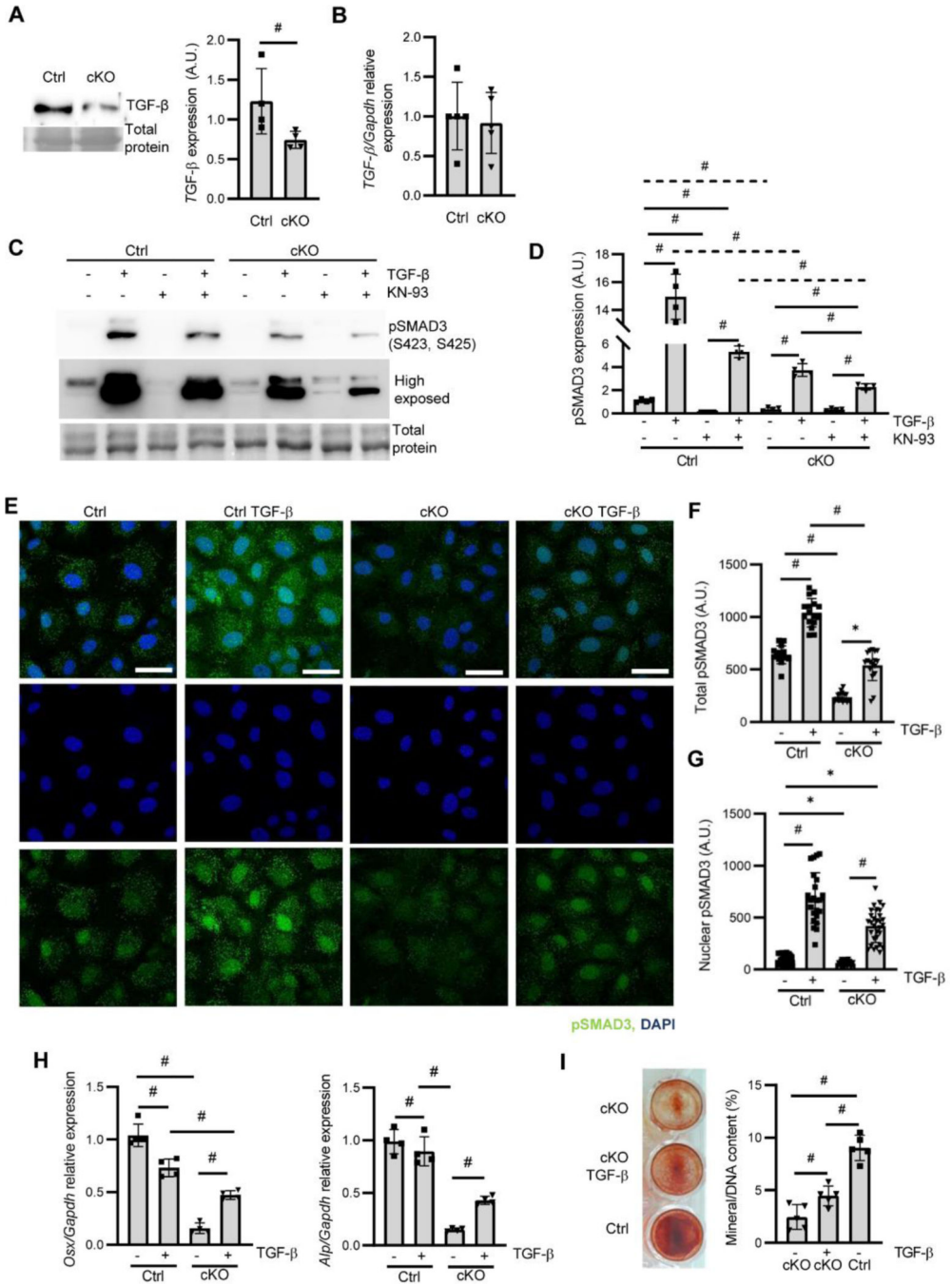

Figure 6: How TRIC-B deficiency impairs SMAD signalling.

(**A**) Western blot analyses of TGF-β level revealed decreased protein in cKO OBs. (**B**) qPCR analyses of TGF-β showed no change in control and mutant cells. (**C**) The SMAD3 phosphorylation level in presence of the CaMKII inhibitor KN93, in absence or presence of exogenous TGF-β, was evaluated by western blot analyses in primary murine OBs. (**D**) Western blot quantification revealed that in control cells pSMAD3 level was increased following TGF-β signalling and, importantly, this effect was abrogated by KN93. pSMAD3 level was partially rescued upon administration of both KN93 and TGF-β treatment. In

mutant murine cells, pSMAD3 level was increased following TGF-β signalling but to a less extend compared to control cells and, importantly, KN93 did not significantly reduced pSMAD3 level. (**E**) Immunofluorescence analyses of pSMAD3. (**F**) Total pSMAD3 level was quantified in control and cKO OB in absence or presence of TGF-β treatment. (**G**) pSMAD3 nuclear localization was analysed in control and cKO OBs in absence or presence of TGF-β treatment. Total and nuclear pSMAD3 level was decreased in cKO and increased by TGF-β treatment but to a lesser extent than treated controls. Nuclei were stained with DAPI. (**H**) qPCR analyses of *Osx* and *Alp* in control and cKO OB at day 7 of culture in absence or presence of 1 ng/mL TGF-β. A partial rescue was found following TGF-β treatment. (**I**) Alizarin red staining of primary cKO OBs cultured in osteogenic medium for 21 days. The cells were untreated or treated with 1 ng/mL TGF-β for 7 days after plating. OBs mineral content was quantified. An increased mineral staining was evident in mutant cells upon treatment, although it did not reach the control level.

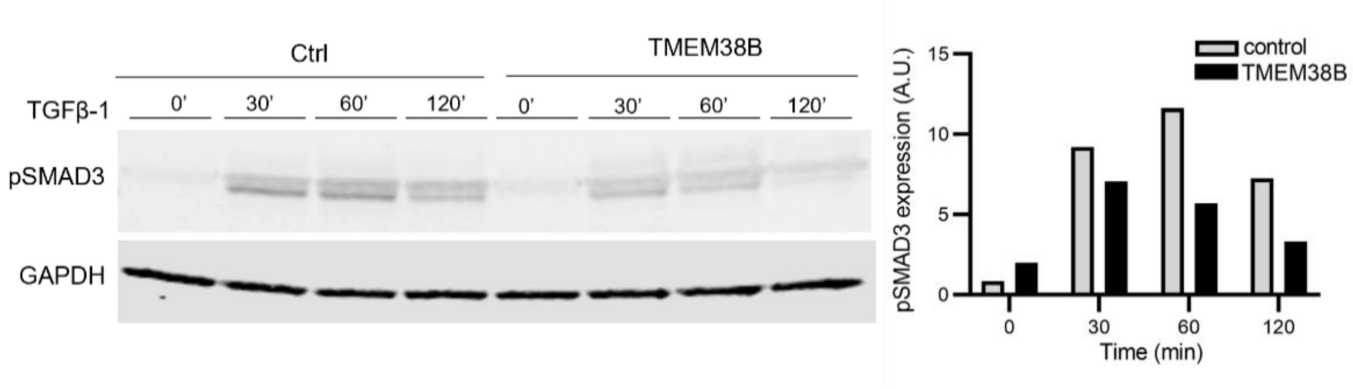

Figure 7: Impairment of SMAD signalling was confirmed in a *TMEM38B*-null OI XIV patient.
Western blot analysis of pSMAD3 in OB from a *TMEM38B*-null OI XIV patient and healthy age-matched control. A reduced pSMAD3 level was found in *TMEM38B*-null OBs upon TGF-β1 treatment, confirming the mouse data. GAPDH was used to normalize protein expression.

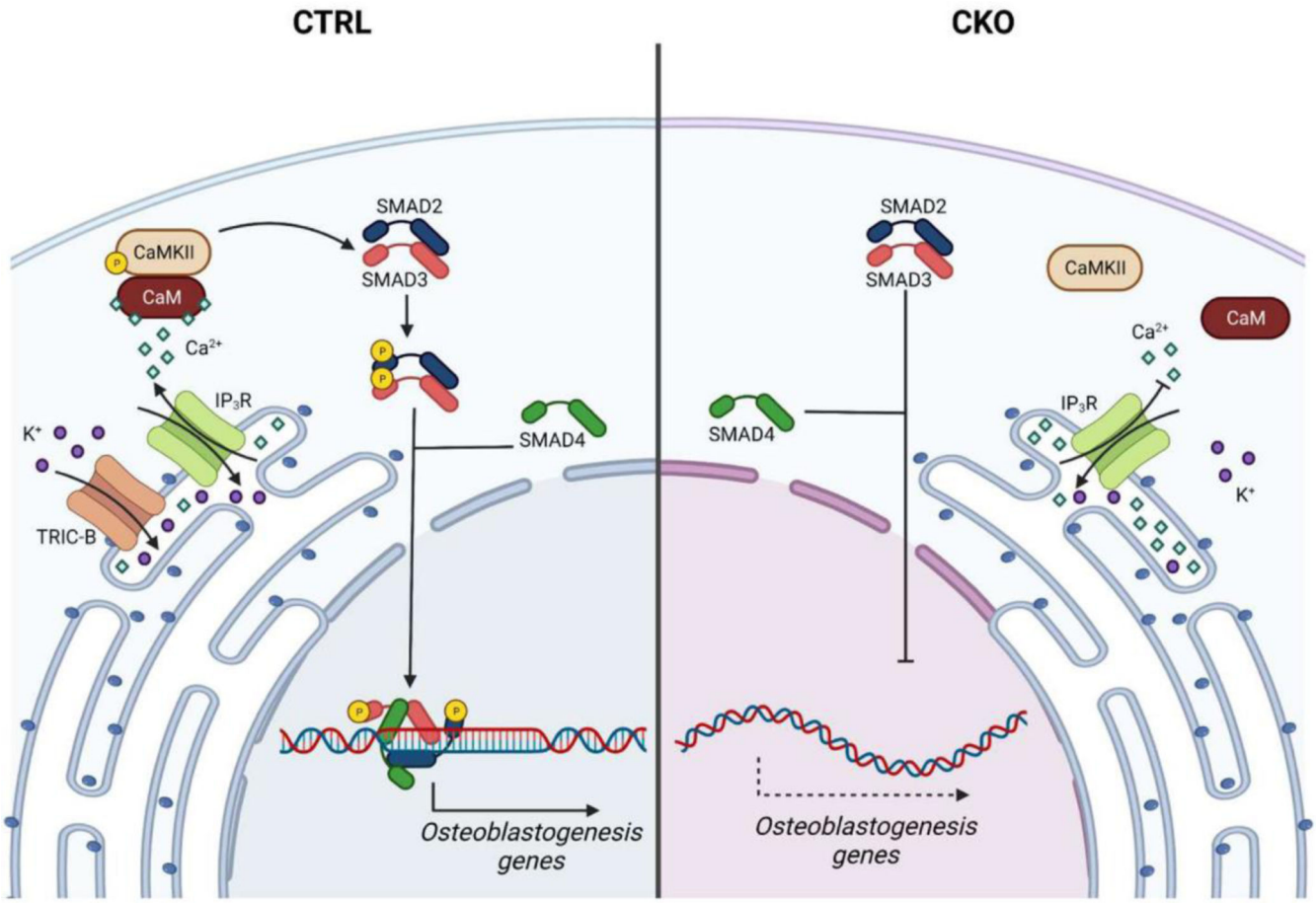

Figure 8: The mechanism behind trimeric intracellular cation channel B function in bone.

When Ca^{2+} fluxes out from the ER to the cytoplasm though the IP3R receptor, it binds CaM and activates the CaMKII that phosphorylates SMAD2 and SMAD3. pSMAD2/3 interact with SMAD4 and the complex translocates to the nucleus where it stimulates transcription of osteoblastogenic genes (*Osx, Alpl, Bglap*). In TRIC-B cKO OBs, in which the mutation causes TRIC-B loss-of-function responsible for an altered Ca^{2+} homeostasis, CaMKII is not activated impairing SMAD signalling and, ultimately, the expression of genes important for the OB development and resulting in the OI phenotype. CaM (calmodulin), CaMKII (calmodulin-dependent kinase II), IP_3R (inositol-3-phosphate receptor), TRIC-B (trimeric intracellular cation channel B). Created by BioRender.com.